NANO LETTERS

Open Access

This article is licensed under CC-BY-NC-ND 4.0

pubs.acs.org/NanoLett

Letter

Epitaxial n-ZnO/MoS_2/p-GaN Heterostructure Light-Emitting Diodes

Imasda Rahmatulloh, Daryll J. C. Dalayoan, Asad Ali, Soobeom Shin, Anh T. D. Nguyen, Taenam Kwon, Satyabrat Behera, Jaehyun Lee, Heekyeong Kim, Hu Young Jeong, Seon Namgung, Gyu-Chul Yi, and Kunook Chung*

Cite This: https://doi.org/10.1021/acs.nanolett.5c06430

Read Online

ACCESS | Metrics & More | Article Recommendations | Supporting Information

ABSTRACT: We investigated an epitaxial strategy for fabricating MoS_2 light-emitting diodes (LEDs). A full-coverage MoS_2 active layer was grown on p-type GaN, and n-type ZnO nanorods were then vertically aligned on the MoS_2 to form a p−n junction with negligible damage to the MoS_2. All materials have nearly matched hexagonal structures, enabling single-crystal alignment. Although the continuous MoS_2 film formed multiple layers (MLs), the ZnO/MoS_2/GaN heterostructure yielded favorable optical characteristics of the ML-MoS_2, including internal quantum efficiency comparable to that of the single-layer MoS_2. The ZnO/MoS_2/GaN LED exhibited stable A and B exciton emissions, which imply direct bandgap transition with spin−orbit coupling. Without mechanically exfoliated or transferred 2D films, this epitaxial approach satisfies the key requirements for fabricating 2D-based optoelectronic and quantum light sources. The strength of epitaxy, such as large-scale scalability and multiple quantum-well formation, will further advance 2D optoelectronics, making them more practical and efficient.

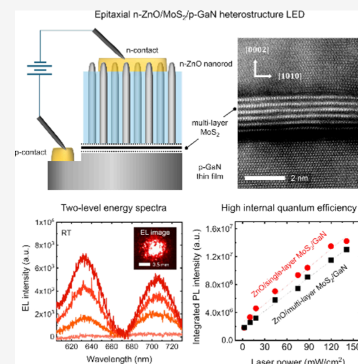

KEYWORDS: *molybdenum disulfide, light-emitting diode, epitaxial heterostructure, gallium nitride, zinc oxide, spin−orbit coupling*

The transition metal dichalcogenide (TMDC) light-emitting diodes (LEDs) have shown promising feasibility for developing high-efficiency wearable optoelectronic devices and quantum light sources.[1−7] The TMDCs, such as MoS_2, are inherently flexible and wearable.[4,7,8] Their bandgaps are in the visible range.[3,9] The direct bandgap transition can be achieved by controlling the layer number or applying an external field to the 2D materials to expect high radiative recombination.[2,9,10] The spin−orbit coupling (SOC) arising from heavy transition metal atoms yields spin splitting of the valence band at the K and K' valleys, which can be utilized for spin-valley locking valleytronics.[2,7,11] There have been various attempts to fabricate high-efficiency TMDC LEDs by using low threading dislocation materials, encouraging the direct bandgap transition, and fabricating the quantum well (QW) heterostructures.[5,10,12−15] These approaches are inspired by conventional semiconductor epitaxy. Still, the fabrication of 2D LEDs has mostly relied on mechanical exfoliation or transfer methods, which hinder the scalability of the device and the fabrication process. To fabricate epitaxial 2D LEDs, one major challenge is finding compatible epitaxial layers to meet the key criteria of single-crystal growth, reliable n-type and p-type doping, and formation of heterostructures and quantum structures with negligible damage in the TMDC materials, while the transfer method is relatively free from these difficulties. Here, we investigated the epitaxial approach to fabricate MoS_2 LEDs by growing the underlying p-GaN film, the intermediate MoS_2 active layer, and the n-ZnO nanorods on top. The monolithic growth of the ZnO/MoS_2/GaN heterostructure was facilitated by the closely matched lattice symmetry and the compatible thermal budgets, ensuring the single-crystal alignments and negligible damage of the MoS_2, respectively. Since ZnO and GaN are wide-bandgap materials, our material design simultaneously satisfies the efficient QW-structured LED.

Unlike conventional monochromatic GaN or GaAs LEDs, the fabrication of TMDC LEDs offers a straightforward method to develop two-level-state optoelectronic devices because of the large valence band splitting in the TMDCs associated with strong SOC.[1,2,11] Since the band splitting occurs at K and K' valleys, the SOC phenomena also signify the direct bandgap transitions,[9,11,16] which are essential to fabricate efficient TMDC LEDs. Strong SOC emissions of the TMDC LEDs have been readily demonstrated using single-layer (SL)- and multilayer (ML)-TMDCs.[10,17] However, previous studies are mostly limited to the use of mechanically exfoliated or transferred TMDCs. The random nature of the exfoliation process results in small and irregular flakes that are hard to extend for fabricating device arrays or wafer-scale integration.[7,18] The 2D film transfer process typically yielded additional labor and cost, material contamination, unavoidable local voids and fluctuations, and environmental instability.[18,19]

Received: December 23, 2025
Revised: April 13, 2026
Accepted: April 17, 2026

Downloaded via ULSAN NATL INST SCIENCE AND TECHLGY on May 4, 2026 at 02:47:49 (UTC).
See https://pubs.acs.org/sharingguidelines for options on how to legitimately share published articles.

ACS Publications

© XXXX The Authors. Published by American Chemical Society

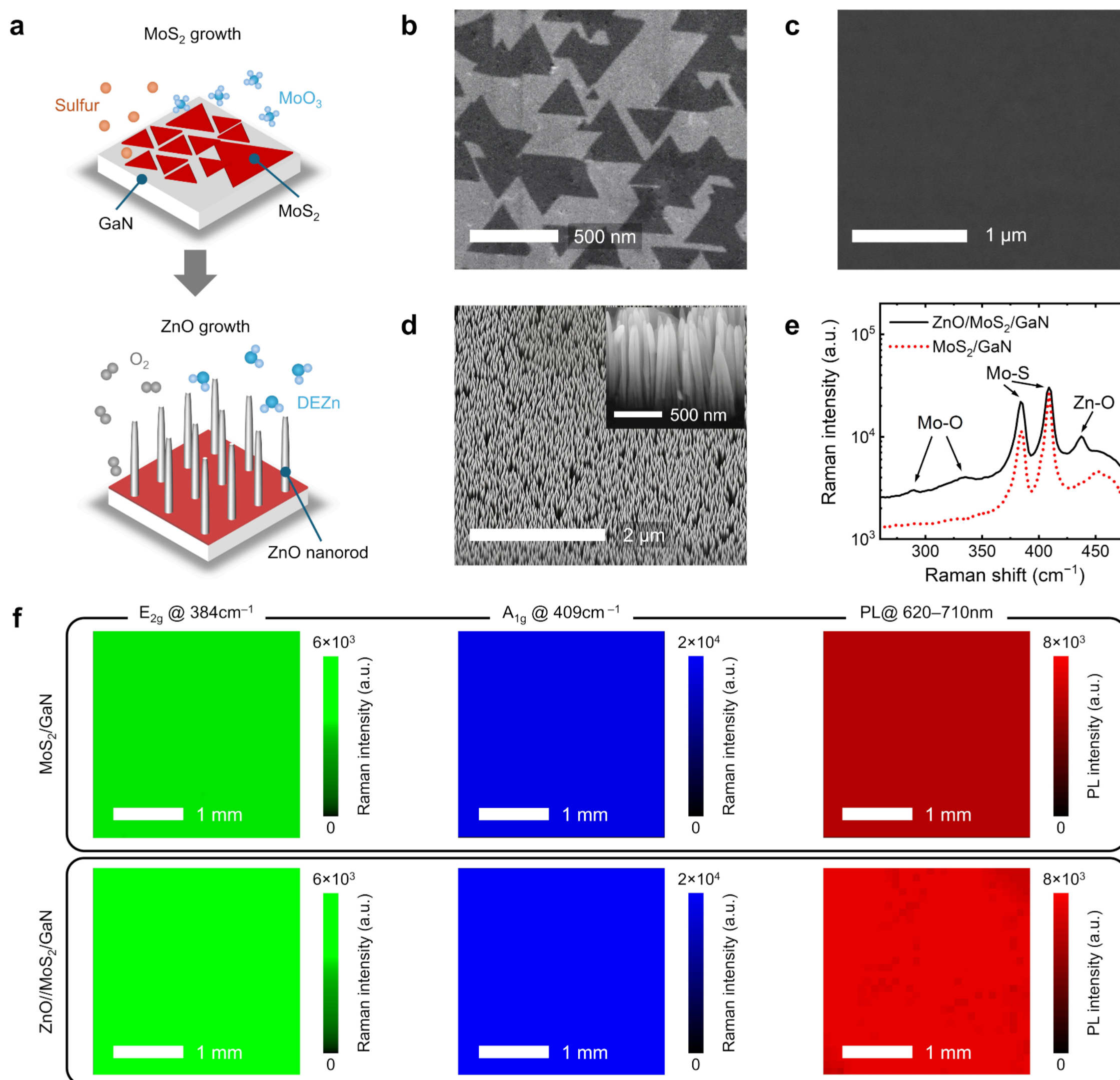

Figure 1. Growth of ZnO/MoS_2/GaN heterostructures. (a) Schematic illustration of the growth process. FE-SEM images of (b) the SL-MoS_2 flakes and (c) the continuous ML-MoS_2 grown on the GaN films. (d) 30°-tilted low- and high-magnification (inset) FE-SEM images of the ZnO nanorods grown on the MoS_2-coated GaN film. (e) Raman spectra of the ML-MoS_2 grown on the GaN film before (red dotted line) and after (black solid line) the ZnO nanorods' growth. (f) Mapping of RT Raman E_{2g} (left) and the A_{1g} (center) peaks and PL intensity (right) of the ML-MoS_2. The top and bottom images show the as-grown ML-MoS_2 on the GaN film and ML-MoS_2 sandwiched by the ZnO nanorods and the GaN film, respectively.

Nevertheless, the poor device scalability can be addressed by growing single-crystal quantum structures and heterostructures with compatible epitaxial layers. In this report, we demonstrated epitaxial n-ZnO/MoS_2/p-GaN heterostructure LEDs obtaining clearly separated two-level energy emissions with a scalable fabrication method and minimal contamination.

To demonstrate MoS_2 LEDs, we fabricate a heterostructure comprising n-ZnO nanorods grown on p-GaN films with an intermediate MoS_2 layer, where the fabrication sequence is illustrated in Figure 1a. ZnO and GaN can be efficient carrier injection layers.[20,21] They are wide-bandgap materials, which allow us to make MoS_2 a QW layer. All components of the heterostructure are hexagonal crystals, and the in-plane lattice constant mismatches are within 2%. Accordingly, a p−QW−n structure MoS_2 LED can be fabricated using epitaxial growth without any transfer process of the 2D film. Moreover, the sequential stack of the heterostructure is designed by thermal budgets of each layer. The typical GaN layers are grown over 1000 °C, while they are merely deteriorated at the MoS_2 growth temperatures of 700−800 °C. Furthermore, high-quality ZnO nanorods can be grown at relatively low temperatures of 500−600 °C, minimizing thermal degradation of the underlying MoS_2.

Figure 1b shows the surface morphology of the MoS_2 layer grown on the planar GaN film. When the MoS_2 growth time was relatively short, discrete triangular SL-MoS_2 flakes were distributed. The in-plane orientations of the MoS_2 flakes exhibit a predominant direction and/or their 180° rotation, while other rotational angles were rarely observed, suggesting that the underlying GaN governed the in-plane crystal orientations of the MoS_2. For LED fabrication, we could not employ SL-MoS_2 because of its discrete formation. However, full-coverage MoS_2 layers can be prepared by increasing the growth time, as shown in Figure 1c, which was further used for the LED active layer. The planar MoS_2 layer is formed on GaN to see negligible contrast differences in the field-emission scanning electron microscope (FE-SEM) image. During the lateral growth, the thickness of the MoS_2 was also increased to

https://doi.org/10.1021/acs.nanolett.5c06430
Nano Lett. XXXX, XXX, XXX−XXX

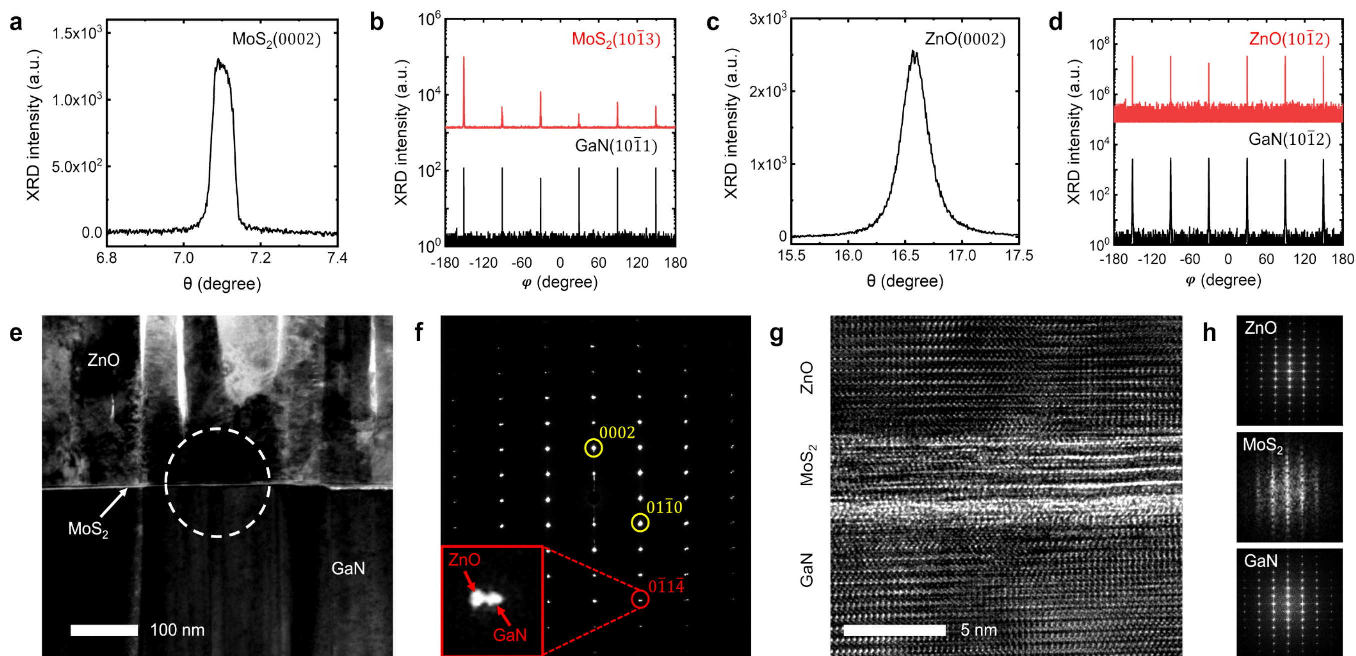

Figure 2. Structural characterization of the ML-MoS_2/GaN and the ZnO/ML-MoS_2/GaN heterostructures. (a) XRD rocking curve of MoS_2 (0002) and (b) the φ-scan of MoS_2 (10$\bar{1}$3) (red solid line) and GaN (10$\bar{1}$1) (black solid line) reflections for the MoS_2/GaN heterostructure. (c) XRD rocking curve of the ZnO (0002) and (d) φ-scan of ZnO (10$\bar{1}$2) (red solid line) and GaN (10$\bar{1}$2) (black solid line) reflections for the ZnO/MoS_2/GaN heterostructure. (e) Cross-sectional TEM image and (f) the corresponding SAED pattern of the ZnO/MoS_2/GaN heterostructure. The white dashed circle in Figure 2e marks the region where the SAED pattern is obtained. The inset of Figure 2f shows the overlapping (0$\bar{1}$1$\bar{4}$) diffraction spots of ZnO and GaN. (g) HR-TEM image of the heterostructure and (h) corresponding fast Fourier transform patterns for ZnO (top), MoS_2 (middle), and GaN (bottom) layers.

become ML. The local thickness of the ML-MoS_2 film ranged from 4 to 11 nm, which corresponds to approximately 5−16 layers. No wrinkles, peeling-off, and residue issues were observed in the surface morphology, suggesting the reliable and clean formation of the MoS_2. After full-coverage growth of ML-MoS_2, ZnO nanorods were grown on the MoS_2-coated GaN layer. As shown in Figure 1d, the ZnO nanorods were vertically well-aligned and exhibited a high growth density of 10^{10} cm^{-2}. The magnified FE-SEM image in the inset of Figure 1d shows that the diameter and the length of the nanorods were measured to be 40 nm and 2.1 μm, respectively. Note that the growth density of the ZnO nanorods was as high as that on 3D single-crystal substrates, such as *c*-Al_2O_3 and Si,[22,23] where the high-density growth feature suggests the feasibility of growing various other overlayers of planar thin films and/or position-controlled nanostructures.[24] The thin film structure can offer a simple device fabrication process and reliable device uniformity in terms of current injection and spreading. The vertically aligned nanostructure arrays enable high-density device integrations and high light extraction/absorption.

Figure 1e shows Raman spectra of the heterostructures before and after the ZnO nanorod growth. The MoS_2/GaN heterostructure exhibited two prominent MoS_2 peaks of the out-of-plane A_{1g} mode at 408.9 cm^{-1} and in-plane E_{2g} mode at 384.5 cm^{-1}. The separation between the two peaks was 24.8 cm^{-1}, indicating ML-MoS_2.[25] Following the ZnO nanorod growth, both A_{1g} and E_{2g} modes remained stable at their original positions. This invariance of Raman shifts suggests the absence of strain in the MoS_2 interlayer.[26,27] We also observed that additional Raman peaks appeared at 287 cm^{-1} and 331 cm^{-1} after the ZnO growth, which are associated with B_{2g} and B_{1g} vibrational modes of Mo−O bonds, respectively.[28] This implies oxygen doping in the MoS_2 layer during ZnO growth. The impurity effects on the ZnO/MoS_2/GaN heterostructure will be discussed further with the PL characteristics in Figure 5.

Figure 1f shows the Raman intensity mapping results of MoS_2 before and after ZnO growth. The E_{2g} and A_{1g} peaks

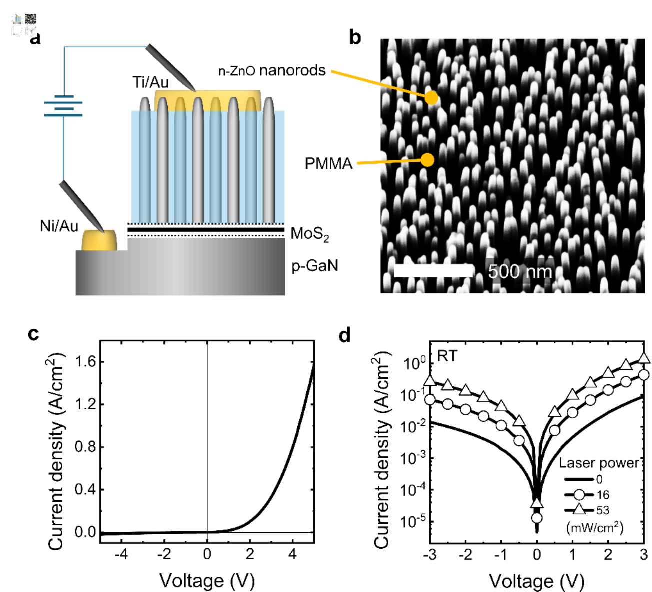

Figure 3. Fabrication of the ZnO/ML-MoS_2/GaN heterostructure LED. (a) Schematic of the device. (b) FE-SEM images of the exposed ZnO nanorod tips surrounded by the PMMA insulating layer. (c) *J*−*V* curve of the device. (d) Logarithmic plot of the *J*−*V* curves under 405 nm-wavelength GaN laser excitations.

https://doi.org/10.1021/acs.nanolett.5c06430
Nano Lett. XXXX, XXX, XXX−XXX

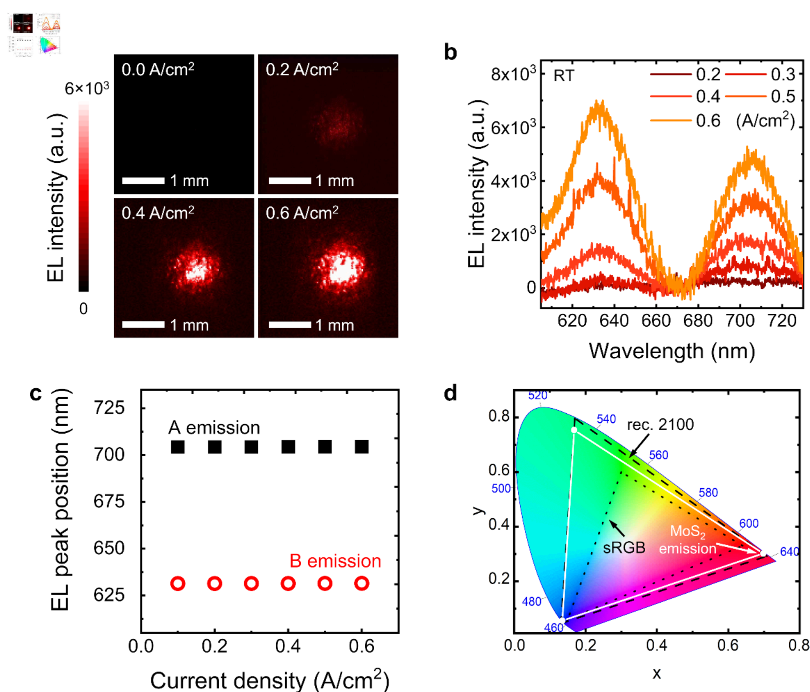

Figure 4. EL characteristics of the ZnO/ML-MoS_2/GaN heterostructure LED. (a) RT light emission images and (b) EL spectra at various applied *J* values ranging from 0.0 to 0.6Acm^{-2}. (c) EL peak positions of A (black solid squares) and B (red open circles) emissions as a function of *J*. (d) Color gamut of the MoS_2 LED for full-color display applications.

were used for the Raman mapping. The room-temperature (RT) PL intensity mapping was conducted with spectral ranges of 620−710 nm. For the as-grown MoS_2 on GaN, both Raman and PL spectra exhibited uniform intensity and spatial distribution. The uniformity remained consistent after ZnO nanorod growth, implying no observable degradations in the MoS_2 layer. One important factor in preserving the MoS_2 layer was the mild growth temperature of the ZnO overlayer. For example, it was hard to fabricate GaN/MoS_2/GaN heterostructures since the MoS_2 layer degraded severely when the growth temperature of the GaN overlayer exceeded 700 °C. Still, the growth temperature was not enough to grow a high-quality GaN overlayer (Figure S1). Additionally, instead of ZnO thin films, we grew ZnO nanorods on MoS_2 for the first epitaxial demonstration, taking several advantages. The growth condition of ZnO nanorods with Ar ambient/carrier gas can be milder than that of the ZnO thin films with H_2 gas.[29,30] The thin film structure generally requires strict lattice and crystallinity conditions at the interface, whereas vertically aligned nanorods can better accommodate a mismatch through their nanoscale geometry. The enhanced light extraction using nanorod structures can offer potential benefits to LED applications.

The crystal orientations and epitaxial relations of the ZnO/MoS_2/GaN heterostructure were examined by X-ray diffraction (XRD). First, we grew 35 nm-thick MoS_2 on a GaN film and obtained rocking curves of the MoS_2(0002) and an azimuthal (φ)-scan of the $MoS_2(10\bar{1}3)$, as shown in Figures 2a and 2b, respectively. The full width at half-maximum (FWHM) value of the rocking curve was 0.05°, which is comparable to that of the high-quality MoS_2 layer.[31,32] The φ-scan of the MoS_2 clearly revealed six-fold rotational symmetry with 60° intervals and in-plane alignments with GaN. Furthermore, we investigated the *c*-axis and in-plane alignments of the ZnO nanorods after we fabricated the ZnO/MoS_2/GaN heterostructure. In Figure 2c, the ZnO(0002) rocking curve exhibited an FWHM of 0.26°, indicating high *c*-axis orientation.[22] Figure 2d shows the six-fold symmetry and the crystal alignments in the φ-scan of ZnO$(10\bar{1}2)$ and GaN$(10\bar{1}2)$. Note that, in the ZnO/MoS_2/GaN heterostructure, the thickness of MoS_2 was 11 nm or below, resulting in very weak XRD intensity to detect. To obtain strong and clear MoS_2 XRD peaks in Figures 2a and 2b, we grew thicker MoS_2 on GaN.

In addition to XRD, transmission electron microscopy (TEM) was employed to investigate microstructural characteristics of the ZnO/ML-MoS_2/GaN heterostructure. Figure 2e shows a low-magnification cross-sectional TEM image of the heterostructure revealing no observable voids or spacing at the heterojunction interface. The selected area electron diffraction (SAED) pattern in Figure 2f and its inset reveal almost identical diffraction spots of ZnO and GaN with a slight separation. Similar to the XRD result, the MoS_2 diffraction peaks were rarely detected in low-magnification TEM. Nevertheless, we confirmed the presence of the ML-MoS_2 interlayer by obtaining the high-resolution transmission electron microscope (HR-TEM) image, as shown in Figure 2g. The clear separation of the morphological signal indicates the formation of the ML-MoS_2 layer between the ZnO and GaN layer. Quantitative measurements show that the interlayer spacings and the atomic spacings for all materials correspond to the (0002) planes and the $(10\bar{1}0)$ planes of their respective layered hexagonal structures (Figure S2), where the spacing of each material agrees with those of the previously reported values.[33−35] The elemental mapping using energy-dispersive X-ray spectroscopy (EDS) also supports the formation of well-defined heterostructures (Figure S3). Figure 2h shows fast Fourier transform patterns of ZnO, MoS_2, and GaN implying single crystallinity. Additionally, we observed stacking faults and blurry diffraction spots for the MoS_2 layer, but these issues

https://doi.org/10.1021/acs.nanolett.5c06430
Nano Lett. XXXX, XXX, XXX−XXX

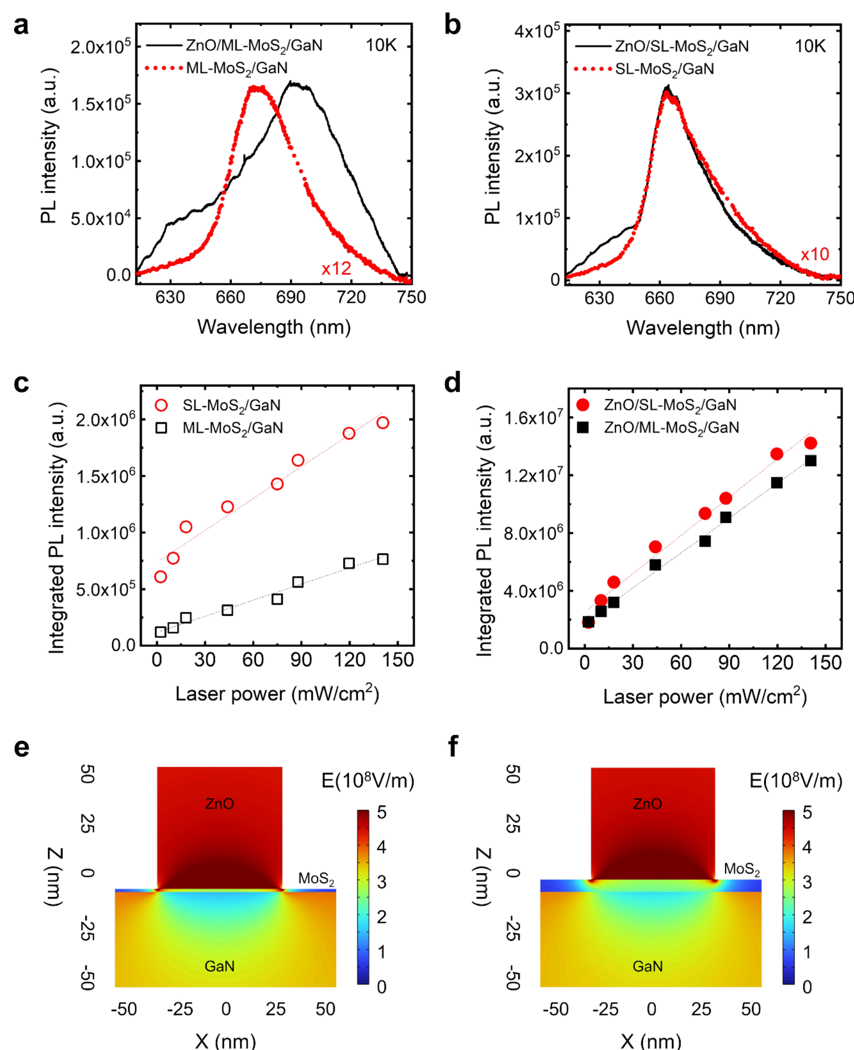

Figure 5. PL characteristics of the MoS_2/GaN and ZnO/MoS_2/GaN heterostructures. Low-temperature PL spectra of (a) ML- and (b) SL-MoS_2-coated GaN before (red dot line) and after (black solid line) ZnO growth under a laser power density of 140 mW cm^{-2}. Integrated PL intensity of the SL- and ML-MoS_2 as a function of laser power density for (c) MoS_2/GaN and (d) ZnO/MoS_2/GaN heterostructures. Simulation results of the built-in electric field for (e) ZnO/SL-MoS_2/GaN and (f) ZnO/ML-MoS_2/GaN heterostructures using the electrostatic module COMSOL.

would eventually be solved by further optimizing the epitaxial growth.

We further fabricated a ZnO/MoS_2/GaN heterostructure LED, as schematically shown in Figure 3a. The LED structure consists of a bottom layer of p-type Mg-doped GaN with a thickness of 1.3 μm, a conformally coated ML-MoS_2 with a thickness ranging from 4 to 11 nm, and vertically aligned ZnO nanorods with a length of 2.1 μm and a density of 1×10^{10} cm^{-2}. All materials, including the p-GaN film, ML-MoS_2, and n-ZnO nanorods, were uniformly grown on the entire substrate, as shown in Figure 1. For carrier recombination in the MoS_2 active region, the p-GaN acts as the hole injection side of the junction, and the ZnO nanorods, which are normally n-type, contribute to electron injections. The heterostructure was partially mesa-etched to form the metal contact of the 50 nm-Ni/20 nm-Au bilayer on the p-GaN layer. To prevent leakage currents, the gaps of the ZnO nanorods were filled with a polymethyl methacrylate (PMMA) insulating layer. The tips of the ZnO nanorods were exposed to form an n-contact. Figure 3b shows an FE-SEM image of the PMMA-coated ZnO nanorods with the exposed tips. The ZnO nanorods maintained their good vertical alignment and uniform distribution. There were no observable voids in the PMMA. Square-shaped n-contact pads were formed on the ZnO tip by depositing a 50 nm-Ti/20 nm-Au bilayer with an area of 500 μm × 500 μm. This contact pad also corresponds to the active device area, where we can inject currents vertically through a ZnO/ML-MoS_2/GaN heterojunction LED.

A clear rectifying behavior was observed in the current density−voltage ($J-V$) curve of the ZnO/ML-MoS_2/GaN heterostructure LED, as shown in Figure 3c. The leakage current was 5×10^{-5}A at −5 V. The turn-on voltage was estimated to be 2 V, which fairly agrees with the bandgap of MoS_2. Additionally, we obtained the $J-V$ curves using a 405 nm-wavelength GaN laser with various laser excitation powers, as shown in Figure 3d. The laser was applied to the back side of the sample, through c-Al_2O_3, p-GaN, MoS_2, and ZnO, with the laser incident normal to the sample surface (Figure S4). Backside direction was chosen because both the c-Al_2O_3 substrate and GaN are transparent at the 405 nm wavelength, while the top side was optically blocked by the relatively thick metal contact. The ZnO/ML-MoS_2/GaN heterostructure LED showed an increased photocurrent for higher laser powers, implying the carrier generations in the MoS_2 working as an

https://doi.org/10.1021/acs.nanolett.5c06430
Nano Lett. XXXX, XXX, XXX−XXX

active layer. For comparison, we also fabricated and obtained *J*−*V* curves of n-ZnO/p-GaN heterostructure LEDs without the MoS_2 interlayer (Figure S5). Except for the MoS_2 growth, the growth and fabrication process were identical for both n-ZnO/p-GaN and n-ZnO/MoS_2/p-GaN LEDs. Unlike those of the n-ZnO/MoS_2/p-GaN LEDs, the n-ZnO/p-GaN LED showed a higher turn-on voltage of 4 V and negligible photocurrent generation under 405 nm laser excitation. This supports that the whole electrical characteristics of ZnO/MoS_2/GaN LEDs are governed by the MoS_2 layer.

The ZnO/ML-MoS_2/GaN heterostructure LED exhibited red emission, as shown in Figure 4a. The gradual increase in the emission intensity for higher current levels implies reliable carrier injection, transport, and radiative recombination in the MoS_2 active layer. However, the LED emitted an additional UV emission around 385 nm (Figure S6), which is only the noticeable competing recombination channel with the MoS_2 emission. We further obtained the band alignment for the n-ZnO/MoS_2/p-GaN heterostructure, where the Fermi level of each material was estimated by previously reported values (Figure S7).[36−38] The heterostructure showed a type-I band alignment. Still, the confinement depth was shallow at the MoS_2/p-GaN interface, which probably resulted in additional UV emissions and a low efficiency of the MoS_2 emissions. Nevertheless, since the bandgaps of GaN and ZnO are wider than that of MoS_2, we believe that this problem can be solved by optimizing the band alignment. For example, the formation of intrinsic ZnO or GaN between the MoS_2/p-GaN interface can be an efficient blocking layer. In this study, we employed a long-pass filter with a cutoff wavelength of 532 nm to obtain the red emissions only. Additionally, we confirmed the red emissions originated from the MoS_2 active layer by obtaining EL spectra of n-ZnO/p-GaN heterostructure LEDs without the MoS_2 interlayer, exhibiting dominant emission at 386 nm and negligible signals in the range of 630−710 nm (Figure S8).

Figure 4b shows the RT electroluminescence (EL) spectra of the ML-MoS_2 LED at different current densities, revealing two dominant emission peaks at 630 nm for the B exciton emission and 705 nm for the A exciton emission. Although the MoS_2 was ML, the peak positions and the two-level-energy spectra strongly suggest direct bandgap transitions in the*K* and *K*′ valleys of ML-MoS_2, where B and A exciton recombination can occur simultaneously due to the split valence band.[10,16] The direct transition of ML-MoS_2 EL emissions was previously reported by other researchers using transfer-based devices.[10] Unlike SL-MoS_2, which has a direct bandgap at the *K* point and therefore can exhibit efficient radiative recombination, ML-MoS_2 possesses an indirect bandgap, with the conduction band minimum located near the Λ valley and the valence band maximum near the Γ hill. Nevertheless, under electrical injections, a strong vertical electric field is established in the ML-MoS_2. This field accelerates injected carriers and enables partial redistribution from the indirect valleys toward the higher-energy *K* valleys, thus activating direct excitonic recombination at *K*. Additionally, the A emission was slightly stronger than the B emission at low *J*, while the B emission became more pronounced for high *J*. The increased B exciton population is presumably due to the A to B exciton transition under high electron injections.[34] As the current density increased, the FWHM values of the A and B emissions decreased from 45 and 38 nm to 35 and 30 nm, respectively, which were narrow enough to signify two distinct spectra for various applied *J*. Figure 4c shows minimal shifts of the EL peak positions with various *J*, implying the negligible quantum-confined Stark effect (QCSE) in this heterostructure LED.

We believe that the epitaxial growth of MoS_2 LEDs, combined with conventional 3D semiconductors, opens a new possibility for advanced optoelectronics. For example, since the MoS_2 LEDs were readily fabricated on the p-GaN layer, we can consider the potential application for GaN-based full-color LEDs. Figure 4d shows the color gamut of our MoS_2 LED for the red pixel and conventional InGaN LEDs for blue and green pixels.[39] The deep red emission of the MoS_2 LED contributes to a broad color triangle (white triangle in Figure 4d) that surpasses the standard RGB LED gamut and approaches the color range of rec. 2100 displays.[39] While InGaN-based red LEDs suffer from a huge QCSE, the negligible QCSE in MoS_2 LED can maintain stable emission wavelengths under varying electrical biases. Moreover, the ZnO/MoS_2/GaN heterostructure LED exhibited A and B emission simultaneously, which provides essential criteria to further control the population of either A or B emissions using various methods including magnetic fields and/or optical polarization.[40−42]

Because of the full-coverage growth, it was unavoidable to use ML-MoS_2 for the LED active layer. Although ML-MoS_2 is known as an indirect bandgap material, the strong feasibility of the direct bandgap transitions was observed in the spin−orbit coupled EL emissions. For this reason, we further investigated the optical characteristics of the MoS_2 layers by measuring the low-temperature PL at 10 K. The PL measurement also enables the comparison of ML-MoS_2 and SL-MoS_2 in the ZnO/MoS_2/GaN heterostructures. The fabrication of SL-MoS_2 LEDs was limited by the difficulty of achieving large-area, continuous SL coverage on the p-GaN. Discontinuities or uncovered regions can result in nonuniform current injections and undesired leakage pathways, preventing reliable carrier recombination within the MoS_2 active layer. Nevertheless, the PL measurement enabled us to obtain SL-MoS_2 emissions in the ZnO/MoS_2/GaN heterostructures.

In Figure 5a, the ML-MoS_2 grown on GaN shows a monochromatic PL spectrum with a dominant peak at 670 nm, which corresponds to the neutral A exciton ($A°$).[25] After the ZnO growth, the dominant PL peak shifted to a longer wavelength of 692 nm, indicating the trion (A^-) peak. Simultaneously, the B emission peak appeared at 630 nm.[43] The A^- peak implies oxygen doping in ML-MoS_2, where the Mo−O bonding Raman peaks were observed for the ZnO/ML-MoS_2/GaN heterostructures, as shown in Figure 1e. However, doping itself rarely affects the B emission enhancement in the ML-MoS_2/GaN heterostructure (Figure S9). A similar PL result was observed for SL-MoS_2, as shown in Figure 5b. The SL-MoS_2 grown on GaN showed a dominant PL spectrum at 664 nm with negligible B exciton emissions, while the B exciton shoulder peak clearly appeared after fabricating the ZnO/SL-MoS_2/GaN heterostructure. The doping effect was rarely observed in the SL-MoS_2. The noticeable B emission enhancement was obtained using the ZnO/MoS_2/GaN heterostructure, where the number of MoS_2 layers and doping effects are less considerable. Additionally, the PL spectra were deconvoluted to distinguish the peak positions of $A°$, A^-, and B excitons (Figure S10). The valence band splitting energy could be estimated to be 100 meV for SL-MoS_2 and 120 meV for the ML-MoS_2. The higher energy separation of the ML-MoS_2 was consistent with the previous reports.[44]

https://doi.org/10.1021/acs.nanolett.5c06430
Nano Lett. XXXX, XXX, XXX−XXX

Moreover, the $ZnO/MoS_2/GaN$ heterostructure yielded much stronger PL intensity, which increased approximately 15 times for ML-MoS_2 and 9 times for SL-MoS_2. The PL intensity is proportional to the laser excitation power, light absorption efficiency, output light collection efficiency, and the internal quantum efficiency. For strong PL intensity under the same laser excitation power, ZnO nanorods can play a major role in enhancing the light absorption and extraction.[45,46] Still, it was interesting that the PL intensity enhancement was larger for ML-MoS_2, implying additional factors of the strong PL intensity. In the $ZnO/MoS_2/GaN$ heterostructure, the oxygen doping was obvious for ML-MoS_2 and minor for SL-MoS_2, while the increased free carrier density in the doped MoS_2 often leads to quenching of the PL intensity rather than its enhancement (Figure S9).[40]

Figures 5c and 5d show the integrated PL intensity of the MoS_2/GaN and $ZnO/MoS_2/GaN$ heterostructures as a function of laser power, respectively. Using the same measurement setup and the material heterostructures, we minimize the effects of light absorption and output light collection efficiencies, where the slope of the PL intensity represents the relative internal quantum efficiency. For the MoS_2/GaN heterostructure, ML-MoS_2 exhibited a 2 times lower gradient compared to that of the SL-MoS_2. This has often been observed in previous reports on thickness-dependent PL due to the reduced probability of radiative recombination arising from its indirect bandgap nature.[25] Nevertheless, the PL intensity slopes of the SL- and ML-MoS_2 became almost identical for the $ZnO/MoS_2/GaN$ heterostructure. This signifies the increased internal quantum efficiency of ML-MoS_2, which is comparable to that of the SL-MoS_2. Since SL-MoS_2 has a direct bandgap, the equivalent quantum efficiency also suggests the direct bandgap transition of the ML-MoS_2 in the $ZnO/MoS_2/GaN$ heterostructure.

According to the previous studies, the ML-MoS_2 can achieve both the SOC phenomena and the direct bandgap transition by applying external electric fields of $0.5-3 \times 10^8$ V m^{-1} perpendicular to the MoS_2 layer.[10,47] The electric field yielded a charge density difference breaking the inversion symmetry in the ML-MoS_2.[48,49] Together with the charge redistribution, the carriers can gain high kinetic energy by the external field, which leads to direct bandgap emissions.[10,49] For the EL measurement, strong electric fields can be applied in ML-MoS_2 by applying the forward bias voltage. It was interesting that PL results also show both SOC emissions and comparable internal quantum efficiency of SL-MoS_2 and ML-MoS_2 in the $ZnO/MoS_2/GaN$ heterostructures because there were no external electric fields for the PL measurement. Meanwhile, ZnO and GaN are polar semiconductors where electric fields over 10^8 V m^{-1} can be induced by their spontaneous polarizations.[50−52] Additionally, we employed the electrostatic form of Maxwell's equation to simulate the built-in electric field in the SL- and ML-MoS_2, as shown in Figures 5e and 5f, respectively. The relative dielectric constants for ZnO, MoS_2, GaN, and Al_2O_3, as well as the spontaneous polarization values for ZnO and GaN, were taken from previous reports.[50,53−55] The induced electric fields were estimated to be $(2-3) \times 10^8$ V m^{-1} at the $ZnO/MoS_2/GaN$ region and below 10^8 V m^{-1} at the ZnO-free region. This suggests the polar semiconductors in the $ZnO/MoS_2/GaN$ heterostructure can generate effective built-in electric fields, enhancing quantum phenomena and efficiency of the ML-MoS_2.

In summary, we demonstrated the fabrication of MoS_2 LEDs by growing n-ZnO/MoS_2/p-GaN heterostructures. By considering the lattice symmetry and the thermal budget, the ML-MoS_2 layer was first grown on the p-GaN film, and then the n-ZnO nanorods were grown on the MoS_2-coated GaN, showing single-crystal alignments of the n-ZnO/MoS_2/p-GaN heterostructure with negligible damage in the MoS_2. The epitaxial ML-MoS_2 LED fully revealed its preferable optical characteristics and quantum phenomena, including direct bandgap transition with strong SOC emissions. Moreover, the 3D surroundings of ZnO and GaN enabled the ML-MoS_2 active layer to have drastically improved internal quantum efficiency and highlight absorption or extraction, suggesting the merit of combining functional 3D materials into the 2D device. This epitaxial approach provides promising feasibility to build reliable 2D devices without using the mechanically exfoliated samples or the 2D film transfer process, which can be further developed to gain higher device efficiency and scalability, such as multiple-QW MoS_2 LED arrays, in a practical manner.

■ ASSOCIATED CONTENT

Supporting Information

The Supporting Information is available free of charge at https://pubs.acs.org/doi/10.1021/acs.nanolett.5c06430.

Supplementary notes containing experimental method details of $ZnO/MoS_2/GaN$ heterostructure LEDs (Note 1); electric field simulation (Note 2); supplementary figures including Raman spectra of GaN grown on MoS_2-coated GaN at different temperatures (Figure S1); TEM analysis of the $ZnO/MoS_2/GaN$ heterostructure (Figure S2); TEM image and corresponding EDS elemental maps of the $ZnO/MoS_2/GaN$ heterostructure (Figure S3); *J*–V measurement setup with 405 nm GaN laser excitation (Figure S4); electrical characteristics of the n-ZnO/p-GaN LED without the MoS_2 active layer (Figure S5); full EL spectra of the ZnO/ML-MoS_2/GaN heterostructure LED (Figure S6); band alignment of the ZnO/MoS_2/p-GaN heterostructure (Figure S7); room temperature EL spectra of the n-ZnO/p-GaN LED without a MoS_2 active layer (Figure S8); optical characterization of oxygen-doped ML-MoS_2 (Figure S9); deconvoluted PL spectra of the SL- and ML-MoS_2 (Figure S10) (PDF)

■ AUTHOR INFORMATION

Corresponding Author

Kunook Chung − *Department of Physics and Graduate School of Semiconductor Materials and Devices Engineering, Ulsan National Institute of Science and Technology (UNIST), Ulsan 44919, Republic of Korea;* orcid.org/0000-0001-7671-8527; Email: kunookc@unist.ac.kr

Authors

Imasda Rahmatulloh − *Department of Physics, Ulsan National Institute of Science and Technology (UNIST), Ulsan 44919, Republic of Korea*

Daryll J. C. Dalayoan − *Department of Physics, Ulsan National Institute of Science and Technology (UNIST), Ulsan 44919, Republic of Korea*

Asad Ali − *Department of Physics & Astronomy, Institute of Applied Physics (IAP), and Research Institute of Advanced*

Materials (RIAM), Seoul National University (SNU), Seoul 08826, Republic of Korea

Soobeom Shin − *Graduate School of Semiconductor Materials and Devices Engineering, Ulsan National Institute of Science and Technology (UNIST), Ulsan 44919, Republic of Korea*

Anh T. D. Nguyen − *Department of Physics, Ulsan National Institute of Science and Technology (UNIST), Ulsan 44919, Republic of Korea*

Taenam Kwon − *Graduate School of Semiconductor Materials and Devices Engineering, Ulsan National Institute of Science and Technology (UNIST), Ulsan 44919, Republic of Korea*

Satyabrat Behera − *Department of Physics, Ulsan National Institute of Science and Technology (UNIST), Ulsan 44919, Republic of Korea*

Jaehyun Lee − *Department of Physics, Ulsan National Institute of Science and Technology (UNIST), Ulsan 44919, Republic of Korea;* orcid.org/0009-0006-4179-8997

Heekyeong Kim − *Graduate School of Semiconductor Materials and Devices Engineering, Ulsan National Institute of Science and Technology (UNIST), Ulsan 44919, Republic of Korea*

Hu Young Jeong − *Graduate School of Semiconductor Materials and Devices Engineering, Ulsan National Institute of Science and Technology (UNIST), Ulsan 44919, Republic of Korea;* orcid.org/0000-0002-5550-5298

Seon Namgung − *Department of Physics, Ulsan National Institute of Science and Technology (UNIST), Ulsan 44919, Republic of Korea;* orcid.org/0000-0002-1730-1665

Gyu-Chul Yi − *Department of Physics & Astronomy, Institute of Applied Physics (IAP), and Research Institute of Advanced Materials (RIAM), Seoul National University (SNU), Seoul 08826, Republic of Korea*

Complete contact information is available at: https://pubs.acs.org/10.1021/acs.nanolett.5c06430

Notes

The authors declare no competing financial interest.

■ ACKNOWLEDGMENTS

This work was supported by the National Research Foundation of Korea (NRF) grant funded by the Korean government (MSIT) (RS-2021-NR061576, RS-2021-NR060087, 2022M3H4A1A04096465, RS-2026-25492893) and Korea Institute for Advancement of Technology (KIAT) grant funded by the Korean Government (MOTIE) (P0023703, HRD Program for Industrial Innovation).

■ REFERENCES

(1) Mak, K. F.; Shan, J. Photonics and Optoelectronics of 2D Semiconductor Transition Metal Dichalcogenides. *Nat. Photonics* **2016**, *10*, 216−226.

(2) Mueller, T.; Malic, E. Exciton Physics and Device Application of Two-Dimensional Transition Metal Dichalcogenide Semiconductors. *npj 2D Mater. Appl.* **2018**, *2*, 29.

(3) Fu, Q.; Hu, Z.; Zhou, M.; Lu, J.; Ni, Z. Excitonic Emission in Atomically Thin Electroluminescent Devices. *Laser Photonics Rev.* **2021**, *15*, 2000587.

(4) Jiang, D.; Liu, Z.; Xiao, Z.; Qian, Z.; Sun, Y.; Zeng, Z.; Wang, R. Flexible Electronics based on 2D Transition Metal Dichalcogenides. *J. Mater. Chem. A* **2021**, *10*, 89−121.

(5) Ahmed, T.; Zha, J.; Lin, K. K. H.; Kuo, H. C.; Tan, C.; Lien, D. H. Bright and Efficient Light-Emitting Devices based on 2D Transition Metal Dichalcogenides. *Adv. Mater.* **2023**, *35*, 2208054.

(6) Thayil, R.; Parne, S. R.; Ramana, C. V. 2D MoS_2 for Next-Generation Electronics and Optoelectronics: From Material Properties to Manufacturing Challenges and Future Prospects. *Small* **2025**, *21*, 2412467.

(7) Patra, C.; Mondal, S.; Mukherjee, R.; Nandakishora, Y. Advanced Synthesis and Unique Properties of 2D Transition Metal Dichalcogenides for Realizing Next-Generation Applications. *ACS Mater. Au* **2025**, *5*, 745−766.

(8) Joseph, S.; Mohan, J.; Lakshmy, S.; Thomas, S.; Chakraborty, B.; Thomas, S.; Kalarikkal, N. A Review of the Synthesis, Properties, and Applications of 2D Transition Metal Dichalcogenides and Their Heterostructures. *Mater. Chem. Phys.* **2023**, *297*, 127332.

(9) Mak, K. F.; Lee, C.; Hone, J.; Shan, J.; Heinz, T. F. Atomically Thin MoS_2: A New Direct-Gap Semiconductor. *Phys. Rev. Lett.* **2010**, *105*, 136805.

(10) Li, D.; Cheng, R.; Zhou, H.; Wang, C.; Yin, A.; Chen, Y.; Weiss, N. O.; Huang, Y.; Duan, X. Electric-Field-Induced Strong Enhancement of Electroluminescence in Multilayer Molybdenum Disulfide. *Nat. Commun.* **2015**, *6*, 7509.

(11) Schaibley, J. R.; Yu, H.; Clark, G.; Rivera, P.; Ross, J. S.; Seyler, K. L.; Yao, W.; Xu, X. Valleytronics in 2D Materials. *Nat. Rev. Mater.* **2016**, *1*, 1−15.

(12) Geim, A. K.; Grigorieva, I. V. van der Waals Heterostructures. *Nature* **2013**, *499*, 419−425.

(13) Withers, F.; et al. Light-Emitting Diodes by Band-Structure Engineering in van der Waals Heterostructures. *Nat. Mater.* **2015**, *14*, 301−306.

(14) Liu, Y.; Weiss, N. O.; Duan, X.; Cheng, H.-C.; Huang, Y.; Duan, X. van der Waals Heterostructures and Devices. *Nat. Rev. Mater.* **2016**, *1*, 1−17.

(15) Uddin, S. Z.; Higashitarumizu, N.; Kim, H.; Rabani, E.; Javey, A. Engineering Exciton Recombination Pathways in Bilayer WSe_2 for Bright Luminescence. *ACS Nano* **2022**, *16*, 1339−1345.

(16) Fan, X.; Singh, D. J.; Zheng, W. Valence Band Splitting on Multilayer MoS_2: Mixing of Spin-Orbit Coupling and Interlayer Coupling. *J. Phys. Chem. Lett.* **2016**, *7*, 2175−2181.

(17) Ma, Y.; Kalt, R. A.; Stemmer, A. Local Strain and Tunneling Current Modulate Excitonic Luminescence in MoS_2 Monolayers. *RSC Adv.* **2022**, *12*, 24922−24929.

(18) Wang, Q. H.; Kalantar-Zadeh, K.; Kis, A.; Coleman, J. N.; Strano, M. S. Electronics and Optoelectronics of Two-Dimensional Transition Metal Dichalcogenides. *Nat. Nanotechnol.* **2012**, *7*, 699−712.

(19) Gao, J.; Li, B.; Tan, J.; Chow, P.; Lu, T.-M.; Koratkar, N. Aging of Transition Metal Dichalcogenide Monolayers. *ACS Nano* **2016**, *10*, 2628−2635.

(20) Park, W. I.; Yi, G.-C. Electroluminescence in n-ZnO Nanorod Arrays Vertically Grown on p-GaN. *Adv. Mater.* **2004**, *16*, 87−90.

(21) Schuster, F.; Laumer, B.; Zamani, R. R.; Magen, C.; Morante, J. R.; Arbiol, J.; Stutzmann, M. p-GaN/n-ZnO Heterojunction Nanowires: Optoelectronic Properties and the Role of Interface Polarity. *ACS Nano* **2014**, *8*, 4376−4384.

(22) Park, W. I.; Kim, D. H.; Jung, S. W.; Yi, G.-C. Metalorganic Vapor-Phase Epitaxial Growth of Vertically Well-Aligned ZnO Nanorods. *Appl. Phys. Lett.* **2002**, *80*, 4232−4234.

(23) Park, W. I.; Yi, G.C.; Kim, M.; Pennycook, S. J. ZnO Nanoneedles Grown Vertically on Si Substrates by Non-Catalytic Vapor-Phase Epitaxy. *Adv. Mater.* **2002**, *14*, 1841−1843.

(24) Ahmed, A.; Chung, K.; Park, W. I.; Yi, G.-C. Methods and Optoelectronic Device Applications of Semiconductor Epitaxy Assisted by Two-Dimensional van der Waals Materials. *J. Inf. Dispersion* **2024**, *25*, 75−95.

(25) Golovynskyi, S.; Irfan, I.; Bosi, M.; Seravalli, L.; Datsenko, O. I.; Golovynska, I.; Li, B.; Lin, D.; Qu, J. Exciton and Trion in Few-Layer MoS_2: Thickness-and Temperature-Dependent Photoluminescence. *Appl. Surf. Sci.* **2020**, *515*, 146033.

(26) Rice, C.; Young, R. J.; Zan, R.; Bangert, U.; Wolverson, D.; Georgiou, T.; Jalil, R.; Novoselov, K. S. Raman-Scattering Measurements and First-Principles Calculations of Strain-Induced Phonon

Shifts in Monolayer MoS_2. *Phys. Rev. B-Condens Matter* **2013**, *87*, 081307.
(27) Conley, H. J.; Wang, B.; Ziegler, J. I.; Haglund, R. F., Jr; Pantelides, S. T.; Bolotin, K. I. Bandgap Engineering of Strained Monolayer and Bilayer MoS_2. *Nano Lett.* **2013**, *13*, 3626−3630.
(28) Tang, J.; et al. In Situ Oxygen Doping of Monolayer MoS_2 for Novel Electronics. *Small* **2020**, *16*, 2004276.
(29) Park, S. I.; Tchoe, Y.; Baek, H.; Heo, J.; Hyun, J. K.; Jo, J.; Kim, M.; Kim, N.-J.; Yi, G.-C. Growth and Optical Characteristics of High-Quality ZnO Thin Films on Graphene Layers. *APL Mater.* **2015**, *3*. DOI: 10.1063/1.4905488
(30) Mao, H.; Gu, S.; Ye, J.; Tang, K.; Gu, R.; Zhu, S.; Huang, S.; Yao, Z.; Zheng, Y. Comparative Study of the Effect of H_2 Addition on Zno Films Grown by Different Zinc and Oxygen Precursors. *J. Mater. Res.* **2015**, *30*, 935−945.
(31) Romanov, R. I.; et al. Synthesis of Large Area Two-Dimensional MoS_2 Films by Sulfurization of Atomic Layer Deposited MoO_3 Thin Film for Nanoelectronic Applications. *ACS Appl. Nano Mater.* **2019**, *2*, 7521−7531.
(32) Španková, M.; et al. Large-Area MoS_2 Films Grown on Sapphire and GaN Substrates by Pulsed Laser Deposition. *Nanomaterials* **2023**, *13*, 2837.
(33) Chen, Z.; Liu, H.; Chen, X.; Chu, G.; Chu, S.; Zhang, H. Wafer-Size and Single-Crystal $MoSe_2$ Atomically Thin Films Grown on GaN Substrate for Light Emission and Harvesting. *ACS Appl. Mater. Interfaces* **2016**, *8*, 20267−20273.
(34) Ou, S.-L.; Yu, F.-P.; Wuu, D.-S. Transformation from Film to Nanorod via a Sacrifical Layer: Pulsed Laser Deposition of ZnO for Enhancing Photodetector Performance. *Sci. Rep.* **2017**, *7*, 14251.
(35) He, Y.; Xiong, H.; Ren, Q.; Chen, Z.; Yu, W.; Liu, J.; Wang, C.; Zhao, J. Enhanced Photoluminescence and Optoelectronic Performance for Wrinkled 2D MoS_2 through Strain Regulation. *Adv. Opt. Mater.* **2025**, *13*, 2500670.
(36) Ding, M.; Zhao, D.; Yao, B.; Li, Z.; Xu, X. Ultraviolet Photodetector based on Heterojunction of n-ZnO Microwire/p-GaN Film. *RSC Adv.* **2015**, *5*, 908−912.
(37) Liu, X.; et al. Band Alignment of ZnO/Multilayer MoS_2 Interface Determined by X-Ray Photoelectron Spectroscopy. *Appl. Phys. Lett.* **2016**, *109*, 071602.
(38) Yan, P.; Cheng, W.; Qi, Y.; Chen, S.; Liao, B.; Ying, M. ZnO Surface Polarity-Modulated Band Alignment and Interface Coupling in 2D-3D MoS_2/ZnO van der Waals Heterojunctions. *Appl. Surf. Sci.* **2026**, *717*, 164805.
(39) García de Arquer, F. P.; et al. Semiconductor quantum dots: Technological progress and future challenges. *Science* **2021**, *373*, No. eaaz8541.
(40) Liu, Y.; Shen, T.; Linghu, S.; Zhu, R.; Gu, F. Electrostatic Control of Photoluminescence from A and B Excitons in Monolayer Molybdenum Disulfide. *Nanoscale Adv.* **2022**, *4*, 2484−2493.
(41) Stier, A. V.; McCreary, K. M.; Jonker, B. T.; Kono, J.; Crooker, S. A. Exciton Diamagnetic Shifts and Valley Zeeman Effects in Monolayer WS_2 and MoS_2 to 65 T. *Nat. Commun.* **2016**, *7*, 10643.
(42) Manca, M.; et al. Enabling Valley Selective Exciton Scattering in Monolayer WSe_2 through Upconversion. *Nat. Commun.* **2017**, *8*, 14927.
(43) Splendiani, A.; Sun, L.; Zhang, Y.; Li, T.; Kim, J.; Chim, C.-Y.; Galli, G.; Wang, F. Emerging Photoluminescence in Monolayer MoS_2. *Nano Lett.* **2010**, *10*, 1271−1275.
(44) Zhang, Y.; Li, H.; Wang, H.; Liu, R.; Zhang, S.-L.; Qiu, Z.-J. On Valence-Band Splitting in Layered MoS2. *ACS Nano* **2015**, *9*, 8514−8519.
(45) Zhang, K.; Zhang, Y.; Zhang, T.; Dong, W.; Wei, T.; Sun, Y.; Chen, X.; Shen, G.; Dai, N. Vertically Coupled ZnO Nanorods on MoS_2 Monolayers with Enhanced Raman and Photoluminescence Emission. *Nano Res.* **2015**, *8*, 743−750.
(46) Kim, M. S.; et al. Enhanced Light Emission from Monolayer Semiconductors by Forming Heterostructures with ZnO Thin Films. *ACS Appl. Mater. Interfaces* **2016**, *8*, 28809−28815.
(47) Klein, J.; et al. Electric-Field Switchable Second-Harmonic Generation in Bilayer MoS_2 by Inversion Symmetry Breaking. *Nano Lett.* **2017**, *17*, 392−398.
(48) Wu, S.; et al. Electrical Tuning of Valley Magnetic Moment through Symmetry Control in Bilayer MoS_2. *Nat. Phys.* **2013**, *9*, 149−153.
(49) Xiao, J.; Long, M.; Li, X.; Zhang, Q.; Xu, H.; Chan, K. S. Effects of van der Waals Interaction and Electric Field on the Electronic Structure of Bilayer MoS_2. *J. Phys.-Condes. Matter* **2014**, *26*, 405302.
(50) Bernardini, F.; Fiorentini, V.; Vanderbilt, D. Spontaneous Polarization and Piezoelectric Constants of III-V Nitrides. *Phys. Rev. B* **1997**, *56*, R10024.
(51) Lähnemann, J.; et al. Direct Experimental Determination of the Spontaneous Polarization of GaN. *Phys. Rev. B* **2012**, *86*, 081302.
(52) Farid, S.; Choi, M.; Datta, D.; Stroscio, M. A.; Dutta, M. Spontaneous Polarization Induced Electric Field in Zinc Oxide Nanowires and Nanostars. *J. Appl. Phys.* **2016**, *119*. DOI: 10.1063/1.4947458
(53) Look, D. C.; Reynolds, D. C.; Sizelove, J. R.; Jones, R. L.; Litton, C. W.; Cantwell, G.; Harsch, W. C. Electrical Properties of Bulk ZnO. *Solid State Commun.* **1998**, *105*, 399−401.
(54) Singh, A.; Lee, S.; Bae, H.; Koo, J.; Yang, L.; Lee, H. Theoretical Investigation of the Vertical Dielectric Screening Dependence on Defects for Few-Layered van der Waals Materials. *RSC Adv.* **2019**, *9*, 40309−40315.
(55) Hatch, K. A.; Messina, D. C.; Fu, H.; Fu, K.; Zhao, Y.; Nemanich, R. J. External Charge Compensation in Etched Gallium Nitride Measured by X-Ray Photoelectron Spectroscopy. *J. Appl. Phys.* **2022**, *131*, 14.

https://doi.org/10.1021/acs.nanolett.5c06430
Nano Lett. XXXX, XXX, XXX−XXX